REFERENCES

1. H. Plaessmsnn, K.G. Yamada, C.E. Rich et al., Sub-nanosecond pulse generation from diode-pumped acoustic-optical *Q*-switched solid-state lasers, Appl Opt 32 (1993), 6616.
2. R. Scheps, J.F. Myers, and G. Mizell, High-efficiency 1.06-μm output in a monolithic Nd:YVO_4 laser, Appl Opt 33 (1994), 5546–5549.
3. Y. Kitaoka, S. Ohmori, K. Yamamoto et al., Stable and efficient green light generation by intracavity frequency doubling of Nd:YVO_4 laser, Appl Phys Lett 63 (1993), 299–301.
4. H.J. Zhang, L. Zhu, X.L. Meng et al., Thermal and laser properties of Nd:YVO_4 crystal, Cryst Res Technol 34 (1999), 1011–1016.
5. G. McConnell, A.I. Ferguson, and N. Langford, Additive-pulse mode locking of a diode-pumped Nd^{3+}:YVO_4 laser, Appl Phys B-Lasers Opt 74 (2002), 7–9.
6. L. Jian, L. Xingqiang, H. Wei et al., High-power diode-pumped high repetitive acousto-optic *Q*-switched intracavity frequency-doubled Nd:YVO_4/KTP green laser, J Chinese J Lasers A27 (2000), 1063–1066 (in Chinese).
7. Y. Chen, Y.P. Lan, and S.C. Wang, Efficient high-power diode-end-pumped TEM_{00} Nd:YVO_4 laser with a planar cavity, J Opt Lett 25 (2000), 1016–1018.
8. W. Changqing, S. Deyuan, L. Jianren et al., Characteristics of LD pumped Nd:YVO_4 laser operating at 1.34 μm, Acta Optica Sinica 17 (1997), 1176–1179 (in Chinese).
9. W. Koechner, Solid-state laser engineering, Science Press, Beijing, 2002, pp. 410–442.

BROADBAND MILLIMETER-WAVE PLANAR ANTENNA ARRAY WITH A WAVEGUIDE AND MICROSTRIP-FEED NETWORK

Soon-Soo Oh,[1] John Heo,[2] Dong-Hyeon Kim,[2] Jae-Wook Lee,[3] Myung-Sun Song,[3] and Young-Sik Kim[2]
[1] Department of Electrical and Computer Engineering
University of Manitoba
Winnipeg, MB R3T 5V6, Canada
[2] Department of Radio Sciences and Engineering
Korea University
Seoul 136-701, Korea
[3] Radio and Broadcasting Research Laboratory
Electronics and Telecommunications Research Institute
Daejeon 305-350, Korea

Received 7 February 2004

ABSTRACT: *In this paper, we describe a fixed-beam broadband planar antenna array at millimeter-wave frequencies. The antenna is fed by waveguide-feed and microstrip-feed networks. In order to ensure fixed beams and a broad bandwidth, a subarray concept is introduced. For efficient coupling, a novel waveguide-to-slot transition consisting of a slot pair and a narrow conductive bar is proposed. Simulated and measured bandwidth is found to be more than 7.1% from 40.5–43.5 GHz. The main beam directions are broadside over all frequencies. The maximum measured antenna gain is 30.2 dBi at 42.0 GHz.* © 2004 Wiley Periodicals, Inc. Microwave Opt Technol Lett 42: 283–287, 2004; Published online in Wiley InterScience (www.interscience.wiley.com). DOI 10.1002/mop.20279

Key words: *planar antenna; waveguide; antenna array; millimeter-wave*

1. INTRODUCTION

With the growth of millimeter-wave communications, especially broadband multimedia wireless services, the demand for a low-cost broadband planar-array antenna has increased. Although microstrip patch antennas with a microstrip-feed network are widely used because of their low fabrication cost, they have serious problems in millimeter-wave large-array applications, such as large feed-line loss and gain degradation [1]. In contrast, slotted-waveguide array antennas have low loss and high efficiency, but high fabrication costs [2]. To obtain both low cost and low loss, standing-wave waveguide/microstrip feed networks have been reported [3, 4]. However, the arrays fed by these standing-wave feed networks have a very narrow bandwidth because the peak position of the E- and H-fields of the standing wave shifts with the operating frequency. Another problem of standing-wave arrays is the frequency-dependent main-beam direction. These characteristics restrict their application within a narrow band [5].

This paper presents a beam-fixed broadband array antenna with high gain operating at 40.5–43.5 GHz. To reduce the feed-line loss, the antenna is fed by a waveguide-feed network in the E-plane direction. The microstrip-feed network is distributed in the H-plane direction in order to decrease fabrication costs. The two feed networks are coupled using the waveguide-to-microstrip transition proposed in this paper. The proposed transition consists of a

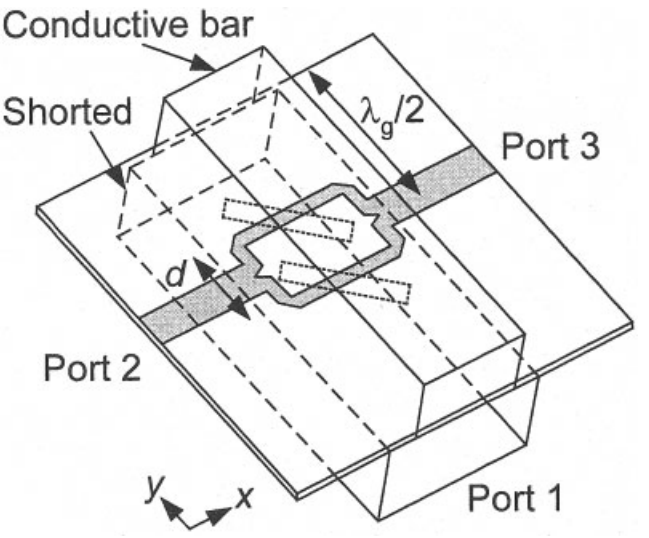

Figure 1 Geometry of the proposed waveguide-to-microstrip transition

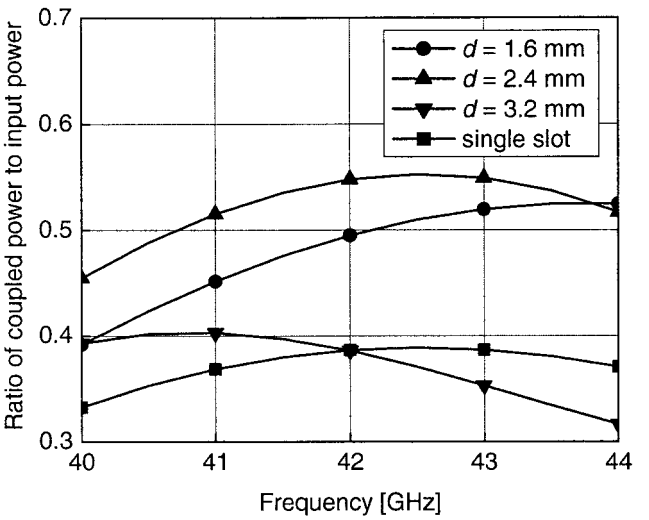

Figure 2 Ratio of coupled power to input power for various spacings *d*

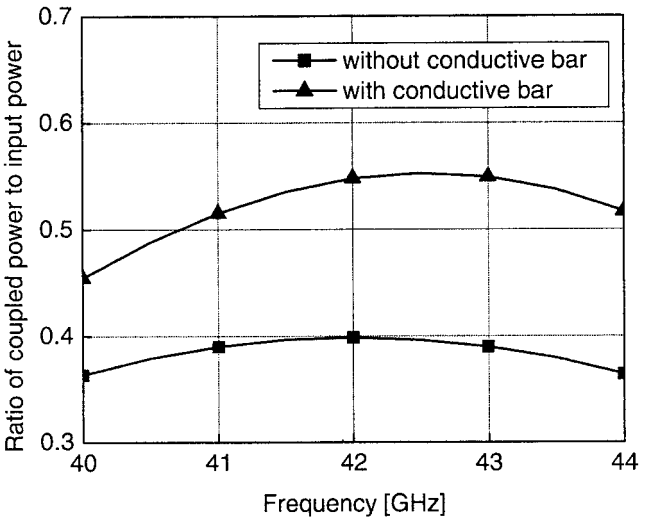

Figure 3 Ratio of coupled power to input power for a slot pair without and with a conductive bar

slot pair and a conductive bar and is more efficient than a conventional transition. We also introduced the subarray concept, which widens the reflection bandwidth and fixes the main-beam direction for variant frequencies. The whole array is divided into four subarrays that consist of eight coupling slots and 30 × 8 antenna elements.

2. SLOT PAIR AND CONDUCTIVE BAR

Figure 1 shows the geometry of the proposed waveguide-to-microstrip transition. The incident wave from Port 1 is coupled through the slot pair and propagates toward Ports 2 and 3 where the microstrip feed network is attached. The slot pair consists of two center-inclined slots that are placed equidistant from the center of the slot pair. The slot is 3.3 mm in length and 0.6 mm in width and is etched on the ground plane of the substrate. The etched ground plane also serves as the upper conductor plate of the waveguide. The dielectric constant of the substrate is 2.2 and its height is 10 mil. Figure 2 shows the ratio of the coupled power to the input power for various slot spacings d. The simulation has been performed using Ansoft's finite-element-method simulator HFSS [6]. The coupled power is calculated as sum of the square of scattering parameter, that is, $|S_{21}|^2 + |S_{31}|^2$. The coupling is dependent on the slot spacing d and the maximum coupling occurs at $d = 2.4$ mm. Figure 2 also shows the coupling power of a single slot, and it is noted that the proposed slot pair with $d = 2.4$ mm couples more power than a single slot. This phenomenon occurs because the slot closer to the shorted wall strongly couples the magnetic field at higher frequencies and the farther slot does the same for lower frequencies.

To increase coupling, we placed a thin, narrow conductive plate, called the conductive bar, 2.0 mm above the slot pair, as shown in Figure 1. The conductive bar is 3.2 mm in width and 0.5 mm in thickness. The cross bar functions as a reflector by redirecting the radiated wave through the slot to the microstrip line. Figure 3 compares the ratio of the coupled power to the input power of the slot pair with and without the conductive bar. More power is coupled with a conductive bar.

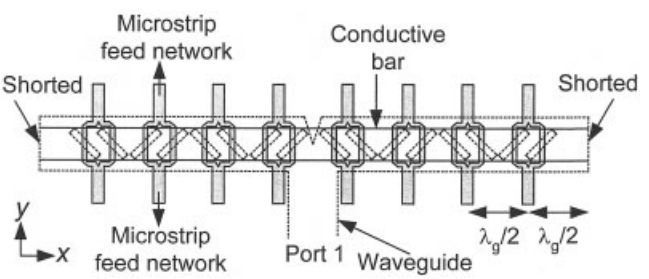

Figure 4 Geometry of a subarray (the microstrip feed network is omitted)

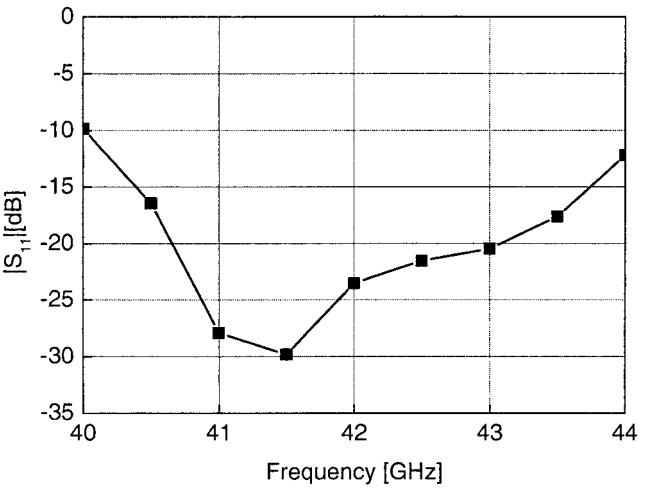

Figure 5 Simulated magnitude of return loss $|S_{11}|$ of a subarray

3. SUBARRAY

A subarray is configured, as shown in Figure 4. The proposed slot pairs are placed a distance of half a guided wavelength, $\lambda g/2$, apart and their orientations are rotated alternately in order to achieve in-phase coupling. The slot pairs closest to the short-circuited wall of the waveguide are also positioned half a guided wavelength from the shorted wall because the slot is a kind of series slot. In the overall array design, the microstrip-feed network with the antenna element will be attached to these slot pairs. The incident wave is split into two feeding waveguides through a T-junction with a triangular ridge. The four slot pairs are placed along one feeding waveguide. This scheme, called the center-feed configuration, is known to have a broader bandwidth than the

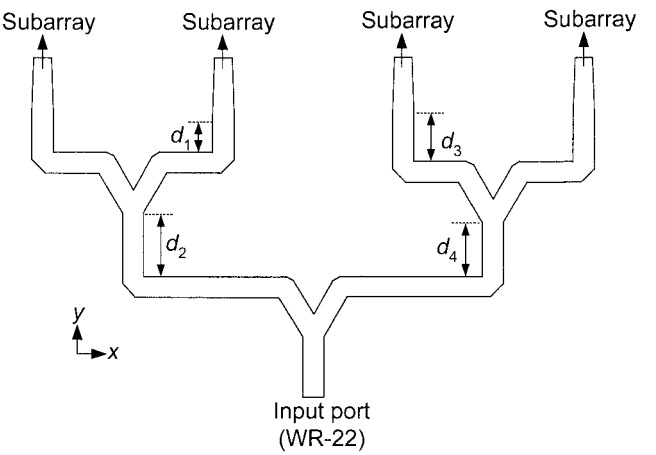

Figure 6 Geometry of the waveguide feed network

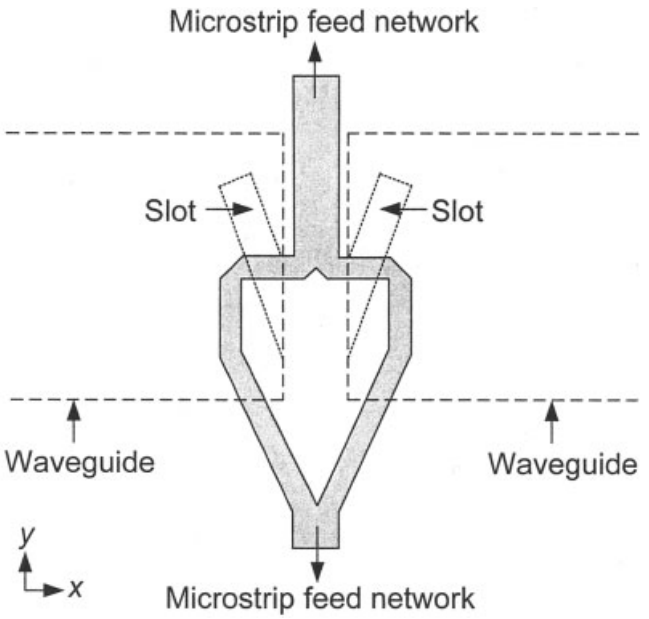

Figure 7 Model with an additional paired slot placed between subarrays

end-feed configuration [6]. We adopted four slots along one feeding waveguide. The particular reason using four slots is that the phase difference of the coupled wave between the first and fourth slots was an endurable quantity as the simulation gave $+32°$ at 40.5 GHz and $-27°$ at 43.5 GHz. A small phase difference means that the deviation of the peak of the wave is small, so that the reflection bandwidth may be broad and the beamwidth is nearly constant from 40.5 to 43.5 GHz. The standard WR-22 waveguide has a dense spacing between antenna elements, which increases the mutual coupling. Therefore, the width of the broad wall of the waveguide was adjusted to 4.8 mm, so that the spacing between slot pairs became 5.3 mm. Figure 5 illustrates the simulated magnitude of the return loss $|S_{11}|$ of the subarray. The bandwidth is nearly 3.5 GHz based on VSWR $\leq$ 1.5. The coupling efficiency calculated from the power of the coupled port is 92.1% at 42.0 GHz. Therefore, the subarray with the slot pair and conductive bar is expected to have a broad bandwidth and high efficiency.

4. FEED NETWORK

4.1. Waveguide Feed Network

Figure 6 shows the waveguide feed network with a WR-22 input port. The Y-junction is designed to have VSWR $\leq$ 1.5 at the desired frequencies. Equal-magnitude, equal-phase waves are fed

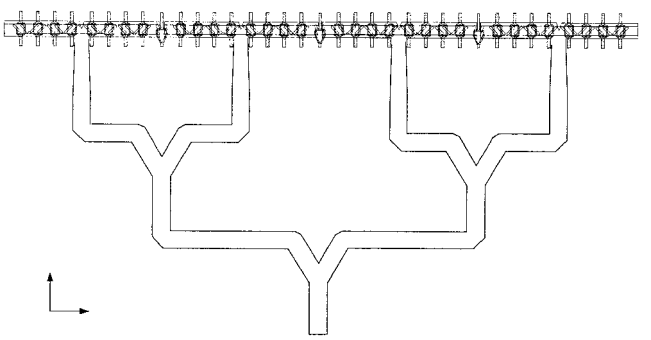

Figure 8 Completed simulation model incorporating Figs. 4, 6, and 7

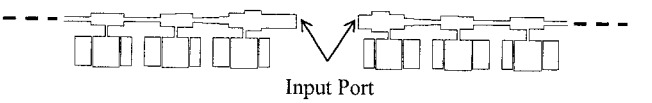

Figure 9 Part of the simulation model of a microstrip feed network with an antenna element

to the subarrays. Although the wave reflected from the junctions and subarrays is small, it becomes severe when it accumulates at the input port. To cancel these reflections, we adjusted the waveguide length, which was $d_1 + d_2 = d_3 + d_4$, but $d_3 - d_1 = d_2 - d_4 = \lambda_g/2$, as shown in Figure 6. The reflected wave is offset due to the half wavelength $\lambda_g/2$ distance.

As shown in Figure 4, the slot pair is placed half a guided wavelength from the shorted end wall, so that the spacing between the marginal elements of each subarray is larger than a guided wavelength, because it is equal to two times half a guided wavelength plus the wall thickness. This broad spacing results in a poor side-lobe characteristic. Therefore, a model with an additional pair of slots is proposed, as shown in Figure 7. Its parameters, such as the microstrip-line length and slot rotation angle, are optimized to be equal magnitude and equal phase, as compared to the neighboring slot pair.

Figure 8 illustrates the complete model based on Figures 4, 6, and 7. From the results of the simulation of Figure 8 and the E-plane pattern of the antenna element, the E-plane radiation pattern is as expected [8].

4.2. Microstrip Feed Network

The microstrip patch with a parasitic patch near the nonradiation edge described in [9] is adopted as the antenna element. The simulation was performed using the method of moments (MoM) tool IE3D [10]. It shows a bandwidth of 3.0 GHz (VSWR $\leq$ 2.1) and a well-formed radiation pattern. The microstrip feed network is designed to have side-lobe level (SLL) of -30 dB using the Dolph–Chebyshev method [8]. Figure 9 shows a partial simulation model consisting of a microstrip-feed network with a patch element. It is impossible to simulate the entire patch and microstrip-feed network simultaneously, so only a 1×30 antenna array was analyzed and the H-plane radiation pattern was examined.

5. SIMULATED AND MEASURED RESULTS

Figure 10 shows a photograph of a fabricated 30×35 array antenna. The substrate is attached to the base plate and secured with many metal screws. A narrow conductive bar is placed

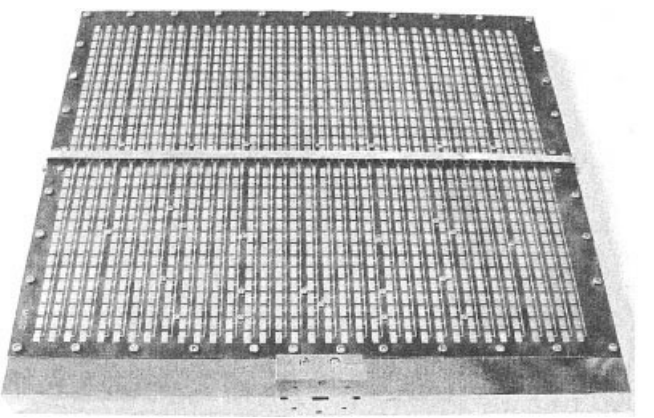

Figure 10 Photograph of a fabricated 30×35 array antenna

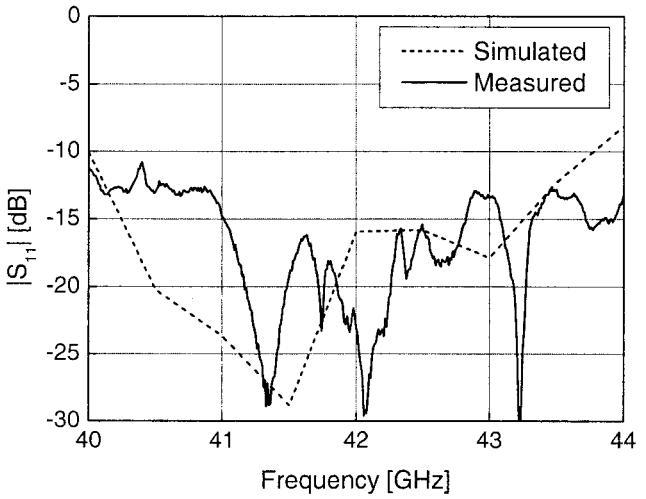

Figure 11 Simulated and measured magnitude of return loss $|S_{11}|$

horizontally along the centerline of the antenna, and fixed to the base plate with screws at the both ends. The whole patch area is 16.0×19.1 cm^2. The measured return loss $|S_{11}|$ is compared with the simulation in Figure 8, as shown in Figure 11. Based on VSWR $\leq$ 2.0, both results shows a broad reflection bandwidth over 3 GHz. The simulated and measured E-plane radiation patterns are plotted in Figures 12(a) and (b), respectively. The SLLs of the simulated patterns at all frequencies are below -12 dB and the measured SLL was also about -12 dB, except at 43.5 GHz. The SLL of about -8 dB at 43.5 GHz may have been due to fabrication tolerance. Figures 12(c) and (d) show the simulated and measured H-plane patterns, respectively. From the measured results, we found that the SLL was about -16 dB, while it was designed to be -30 dB. The reduction from the design goal is caused by the fabrication tolerance and mutual coupling between the antenna elements and microstrip feed network. Figure 12 shows that the beam widths of the E-plane pattern are almost 2.0° over all operating frequencies. This is because the subarray is configured in the E-plane direction. In contrast, the beam widths of the H-plane become broad, as the frequency is far from the center frequency, which is due to the center-feed configuration of the

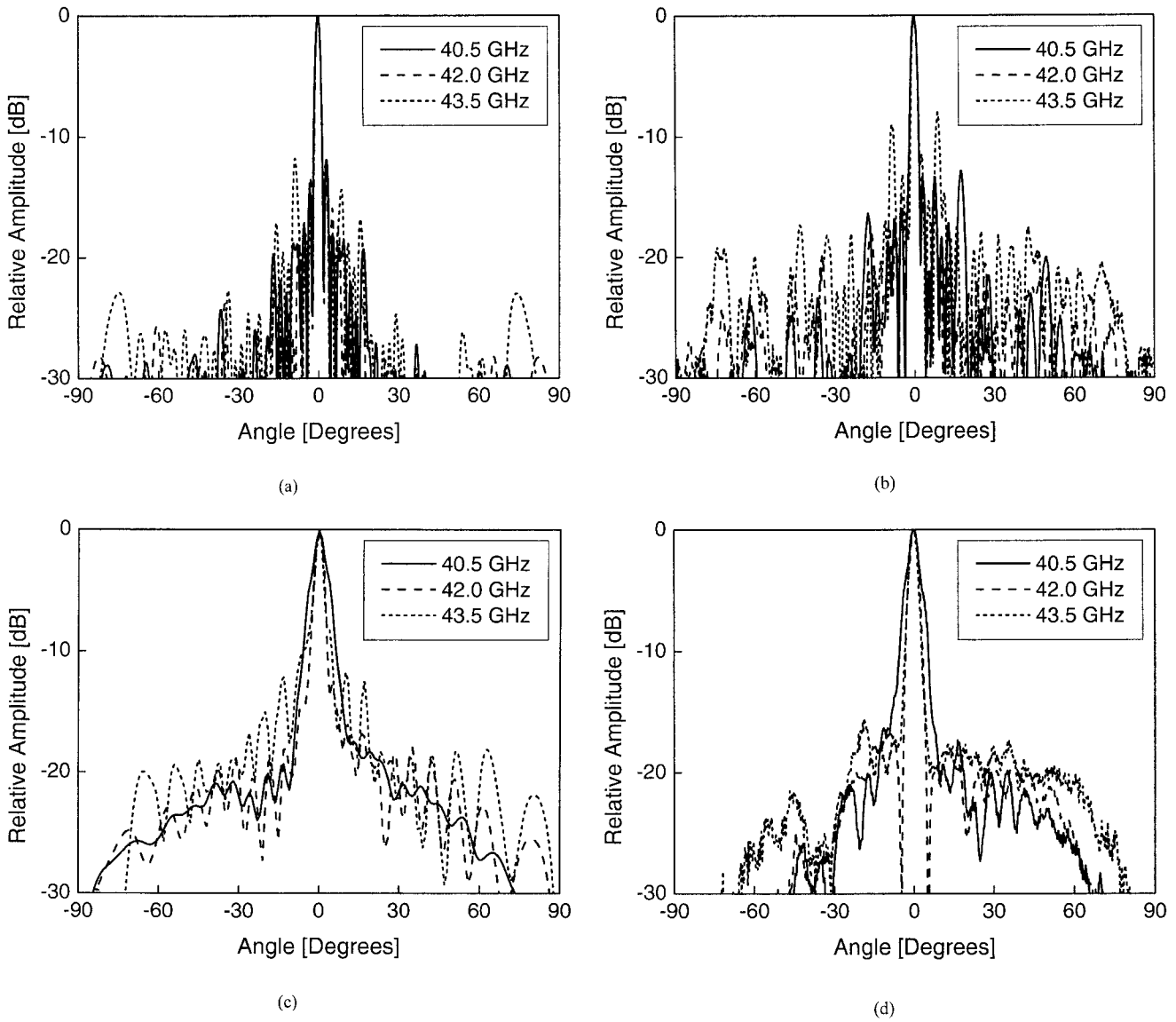

Figure 12 Radiation patterns: (a) simulated and (b) measured E-plane; (c) simulated and (d) measured H-plane

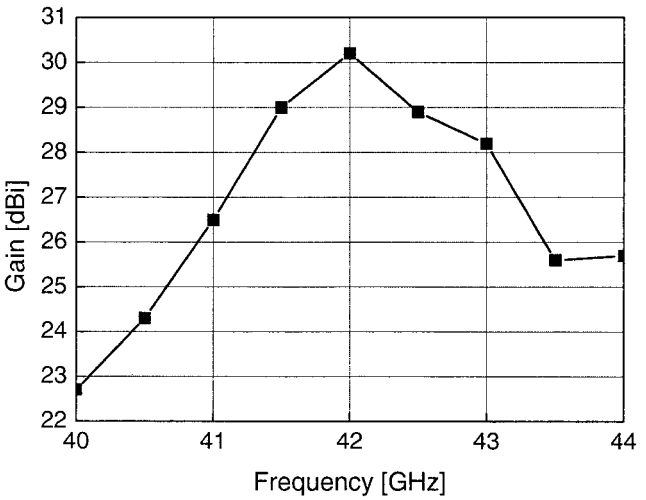

Figure 13 Measured antenna gain

H-plane direction. The measured antenna gain is plotted in Figure 13. At the center frequency of 42.0 GHz, it has a high gain of 30.2 dBi. However, degradation of about 8 dBi can be observed, as compared to the theoretical aperture gain. This is believed to be due to imperfect electrical contact between the ground plate of the substrate and the waveguide [11]. This can be overcome by using chokes [11]. Another reason for this is the inherent conductor loss of the microstrip feed network [1].

6. CONCLUSION

In this study, a 30 × 35 millimeter-wave planar array antenna has been designed. The array is fed by a waveguide-feed network to reduce the feed-line loss and by a microstrip-feed network to reduce the cost. A subarray was introduced with fixed beams and broadband characteristics. A novel waveguide-to-microstrip transition was proposed, so that strong coupling occurred over the desired frequencies. The fabricated antenna has a reflection bandwidth of over 3.0 GHz (VSWR ≤ 2.0). SLLs below −12 dB in the E-plane are seen at all frequencies, except 43.5 GHz, while they are below −16 dB in the H-plane. The measured antenna gain is 30.2 dBi. The deterioration in pattern and gain can be improved by a perfect electrical contact or a choke. Finally, the proposed antenna array can be successfully applied to broadband millimeter-wave communication services.

REFERENCES

1. F.K. Schwering, Millimeter wave antennas, Proc IEEE 80 (1992), 92–102.
2. Y. Kimura, K. Fukazawa, J. Hirokawa, M. Ando, and N. Goto, Low-sidelobe single-layer slotted waveguide arrays at 76 GHz band, IEICE Trans Commun E84-B (2001), 2377–2386.
3. F.P.V.D. Wilt and J.H.M. Strijbos, A 40-GHz planar array antenna using hybrid coupling, Perspectives on radio astronomy: Tech for large antenna arrays, Dig (1999), 129–134.
4. F. Kolak and C. Eswarappa, A low-profile 77-GHz three-beam antenna for automotive radar, IEEE Microwave Theory Tech Soc Int Symp Dig, Phoenix, AZ, (2001), 1107–1110.
5. M. Hamadallah, Frequency limitations on broadband performance of shunt slot arrays, IEEE Trans Antennas Propagat 37 (1989), 817–823.
6. Ansoft Corp., HFSS 8.0, PA, 2001.
7. M. Müller, I.P. Theron, and D.B. Davidson, Improving the bandwidth of a slotted waveguide array by using a centre-feed configuration, IEEE Microwave Theory Tech Soc Int Symp Dig, Los Angeles, CA, (1999), 1075–1080.
8. W.L. Stuzman and G.A. Thiele, Antenna theory and design, Wiley, New York, 1998.
9. S.S. Oh, S.H. Seo, M.K. Yoon, C.Y. Oh, E.B. Kim, and Y.S. Kim, A broadband microstrip antenna array for LMDS applications, Microwave Optical Tech Lett 32 (2002), 35–37.
10. Zeland Software, Inc., IE3D 6.0, New York, 1999.
11. Y. Kimura, K. Fukazawa, J. Hirokawa, and M. Ando, Alternating-phase fed single-layer slotted waveguide arrays with chokes dispensing with narrow wall contacts, IEE Proc Microwave Antennas Propagat 148 (2001), 295–301.

A 3-mW CONCURRENT 2.4/5.2-GHz DUAL-BAND LOW-NOISE AMPLIFIER FOR WLAN APPLICATIONS IN 0.18-μm CMOS TECHNOLOGY

Tai-Hsing Lee and Yo-Sheng Lin
Department of Electrical Engineering
National Chi-Nan University
Puli, Taiwan, R.O.C.

Received 5 February 2004

ABSTRACT: *A concurrent 2.4/5.2-GHz dual-band monolithic low-noise amplifier implemented with a 0.18-μm mixed-signal CMOS technology is reported for the first time. This LNA only consumed 3-mW power, and achieved minimum noise figures of 3.3 and 3.26 dB and 2.4 and 5.2 GHz, respectively. Input and output return losses more than 10 dB were obtained at both 2.4 and 5.2 GHz. In addition, IIP3 of 17 and 5 dBm were achieved at 2.4 and 5.2 GHz, respectively. No off-chip components were required for input and output matching. To our knowledge, this LNA exhibits a state-of-the-art performance. Due to the careful selection of the size of the transistors and the passive elements in our proposed method power matching and noise matching can be achieved simultaneously at the dual-band of interest.* © 2004 Wiley Periodicals, Inc.
Microwave Opt Technol Lett 42: 287–292, 2004; Published online in Wiley InterScience (www.interscience.wiley.com). DOI 10.1002/mop.20280

Key words: *concurrent; dual band; CMOS; LNA*

1. INTRODUCTION

Wireless communication has evolved into a world of multistandards/multiservices with operating frequencies of 900 MHz/1.8 GHz/1.9 GHz for GSM, 1.5 GHz for GPS, and 2.4/5.2/5.7 GHz bands for WLAN [1, 2]. Therefore, it is desirable to combine two or more standards in one mobile unit. Conventional multiband transceivers (the so-called nonconcurrent transceivers), which can operate at multiple different bands, are achieved by switching between multiple independent signal paths. The multiband transceivers solution inevitably confronts some serious problems. For example, the cost will be increased due to additional signal path, die size, and power consumption. In addition, meticulous frequency planning is also an important issue. In this paper, we report a dual-band LNA based on the concurrent dual-band receiver architecture [3], which is capable of simultaneous operation at two different frequencies without consuming double power or significantly increasing of the die size. If we elaborately choose the size and transconductance of the transistors and the layout of the passive elements, the source impedance ($R_{opt} + jX_{opt}$), which corresponds to the minimum noise-figure condition, can be very